

Interference between Rayleigh, Delbruck, and nuclear resonance scattering processes

Sylvian Kahane, R. Moreh, and O. Shahal
Nuclear Research Center, Negev, Beer-Sheva, Israel
and Ben-Gurion University of the Negev, Beer-Sheva, Israel
 (Received 25 May 1983)

The forward scattering cross section at $\theta=1^\circ$ and 1.7° of $E=4-10$ MeV monoenergetic photons from Pb and Bi targets has been measured. The photon beam was obtained from the $\text{Fe}(n,\gamma)$ reaction. The elastic cross section at such angles, being dominated by Rayleigh and Delbruck scattering processes, was measured relative to the Compton cross section. The fact that one of the γ lines of the $\text{Fe}(n,\gamma)$ reaction happens to overlap the 7.28 MeV level in ^{208}Pb , yielding a strong nuclear resonance fluorescence signal, enabled us to observe, for the first time, an interference effect with the Rayleigh and Delbruck scattering processes. A theoretical expression of the nuclear resonance scattering amplitude for the specific case of the random photoexcitation process is derived. The interference effect of this latter process with Rayleigh and Delbruck scattering is calculated and an excellent agreement with measured values is obtained.

[NUCLEAR REACTIONS Pb, ^{208}Pb , $^{209}\text{Bi}(\gamma,\gamma)$, $E=4.2-9.3$ MeV, measured
 $\sigma(\theta)$, Delbruck and Rayleigh scattering, nuclear resonance fluorescence, interference effects.]

I. INTRODUCTION

A series of studies of the elastic scattering of photons has been carried out in our laboratory over the past few years.¹⁻⁶ In these studies monoenergetic photon beams $E=4-10$ MeV generated from the (n,γ) reaction were usually employed, and involved two main categories of experiments. In the first,^{1,2,7} isolated nuclear levels were photoexcited by a chance overlap between one of the incident (n,γ) lines of the photon beam ($\Delta E_i \sim 10$ eV) and a Doppler-broadened nuclear level ($\Delta E_r \sim 10$ eV). The elastic scattering, namely the nuclear resonance fluorescence (F) from these isolated levels (together with some inelastic transitions), were thus studied in detail. The differential scattering cross sections (at $\theta \gtrsim 90^\circ$) occurring in such measurements are in the 10 mb/sr to 1 b/sr range and are usually much higher than the cross sections occurring in the second category of measurements³⁻⁶ where four coherent fundamental scattering processes are involved, namely nuclear Thomson (T), nuclear resonance (N), Rayleigh (R), and Delbruck (D) scattering. Thus in F measurements the contribution of the fundamental scattering processes can normally be ignored at $\theta \gtrsim 90^\circ$. However, with the advent of forward-angle elastic scattering measurements,⁶ where the cross sections are dominated by the R and D contributions, it became feasible to observe possible interference effects between F with R and D scattering. This is because the differential cross section of R and D scattering at $\theta \sim 1^\circ$ and $Z \gtrsim 50$ is about $\gtrsim 100$ mb/sr and hence comparable to the F cross sections. It should be emphasized that the contribution of the other nuclear resonance (N) process, arising from the effect of the giant dipole resonance (GDR), together with that of the T scattering process, is very small at $E \sim 8$ MeV. In fact, the combined cross section of these two processes at $\theta \sim 1.5^\circ$ is smaller by $\sim 10^4$ compared to that of F , D , and

R scattering processes, and is thus ignored in what follows.

In the present work we employed a $\text{Fe}(n,\gamma)$ source together with a Pb target because ^{208}Pb is known to scatter by chance the 7.28 MeV line of the $\text{Fe}(n,\gamma)$ reaction, yielding one of the most intense F signals reported in the literature.⁸ This scattering event is thus suited for such interference studies, first because the high Z of the ^{208}Pb target ($Z=82$) yields high R and D scattering cross sections at small angles, and second, it is possible to compare the elastic scattering of the 7.28 MeV line with other γ lines, close in energy, where no F process contributes. Third, the Pb scattering results can be compared with those from a Bi target ($Z=83$), thus yielding more reliable information concerning the interference process.

In the past, an extensive study was carried out concerning the contribution to elastic scattering of each of the four coherent processes. This was done by selecting the photon energies, the scattering angles, and the Z of the target in such a way as to enhance one process at a time while minimizing the others. In addition, interference effects between pairs of scattering processes, T and N , R and D , and N and D , were all clearly observed.^{4-6,9,10} However, the interference between the F and other processes was ignored.⁹ In all these measurements, the overall agreement between experiment and calculations obtained using the existing scattering amplitudes, were usually much better than the 10% level. In the present work, a new interference effect between the F and R and D scattering amplitudes is presented together with the complete theoretical treatment; a good agreement between calculated and measured values was obtained.

II. EXPERIMENTAL DETAILS

The photon beam (Fig. 1) was produced by the (n,γ) reaction on five iron disks (each 3 cm thick by 8 cm in di-

ameter and separated by 3 cm) placed along a tangential beam tube and near the core of the IRR-2 reactor. The γ beam was collimated and neutron filtered before hitting the scatterer. Typical intensities of the strong γ lines are 10^6 photons per cm^2 on the target.

To achieve small forward scattering angles, we employed a shadow beam geometry shown in Fig. 1 and described in more detail elsewhere.⁶ The scattering angle could be varied by changing the diameter of the absorber C , the scatterer-detector distance, and the total thickness of the collimator. In this manner scattering angles of $\theta \sim 1^\circ$ and 1.7° were obtained. One of the most important experimental points in such measurements is to reduce the spurious scattering signal arising from the outer edges of the absorber, from the inner walls of the collimator, and mainly from a misalignment of the whole system. The scattering angles were determined from the energy separation between the elastic and the Compton scattered photons and were found to be $\theta = 0.95^\circ \pm 0.07^\circ$ and $1.69^\circ \pm 0.02^\circ$. The angular spread of the scattered radiation as determined from the width of the Compton scattered peaks was $\Delta\theta = 0.84^\circ \pm 0.03^\circ$. Ring targets of natural Pb (6 cm outer diameter and 4.65 g/cm^2 thick) and Bi (6 cm outer diameter and 4.51 g/cm^2 thick) were employed. The background contributed by the edges of the collimator and the absorber was measured by removing the ring target. In addition, the shape of the Compton scattered peaks were obtained by replacing the Pb target by a low- Z target such as Al or C which contained an equivalent number of scattering electrons.

III. THEORETICAL REMARKS

A. Differential elastic scattering cross section

The *coherent* differential elastic scattering cross section may be written in terms of linearly polarized waves as

$$\frac{d\sigma}{d\Omega} = \frac{1}{2} r_0^2 (|A_{\parallel}|^2 + |A_{\perp}|^2), \quad (1)$$

where A_{\parallel} and A_{\perp} are the scattering amplitudes polarized parallel to and perpendicular to the scattering plane. Each is a coherent superposition of D , R , F , N , and T scattering amplitudes. As pointed out above, the contribution of N and T scattering processes is negligible at small θ and high Z , and hence we may write

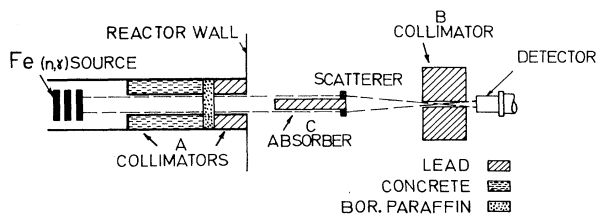


FIG. 1. Schematic diagram (not to scale) of the experimental system. The dimensions of the iron absorber C were 100 cm long, 4 cm in diameter (for $\theta \sim 1.7^\circ$), and 3 cm in diameter (for $\theta \sim 1.0^\circ$). The dimensions of the lead collimator B were 2 cm diameter by 30 to 40 cm long (depending on the value of θ). The scatterer-detector distance was ~ 135 cm.

$$\begin{aligned} A_{\parallel} &= A_D^{\parallel} + A_R^{\parallel} + A_F^{\parallel} = A_S^{\parallel} + A_F^{\parallel}, \\ A_{\perp} &= A_D^{\perp} + A_R^{\perp} + A_F^{\perp} = A_S^{\perp} + A_F^{\perp}, \end{aligned} \quad (2)$$

where the subscript S corresponds to the combined coherent amplitude of $(D+R)$ scattering.

In general each amplitude is complex; for example,

$$\begin{aligned} A_F^{\parallel} &= A_{F1}^{\parallel} + iA_{F2}^{\parallel}, \\ A_F^{\perp} &= A_{F1}^{\perp} + iA_{F2}^{\perp}. \end{aligned} \quad (3)$$

We hereby discuss each scattering amplitude separately. Since the effect of the F scattering amplitude was never treated in the literature, it will be discussed here in some detail.

B. Rayleigh amplitudes

R scattering deals with the contribution of bound atomic electrons to the elastic scattering of photons. This process is very complicated to calculate. In recent years, satisfactory tables and codes have emerged from the work of the Pittsburgh group.¹¹ These results were limited to photon energies below 1 MeV and to K - and L -shell electrons. In the range of momentum transfers appearing in the present work, namely $x < 10 \text{ \AA}$, the R amplitudes are approximated by the modified form factors¹² calculated using the Hartree-Fock-Slater relativistic wave functions of Liberman *et al.*¹³:

$$g(q, Z) = 4\pi \int \eta(r) \frac{\sin(qr)}{qr} \frac{mc^2}{mc^2 - E_B - V(r)} r^2 dr, \quad (4)$$

where

$$q = (E/c) \sin(\theta/2)$$

is the momentum transfer, E_B is the electron binding energy, $\eta(r)$ is the density of the electron cloud, and $V(r)$ is the Hartree-Fock-Slater mean potential of the electron. Table I lists the R amplitudes calculated using Eq. (14) for energies in the range $E = 4-10.0$ MeV for both Pb and Bi at $\theta = 1^\circ$ and 1.7° .

It may be noted that the R amplitudes listed in Table I differ by not more than 5% at 6.0 MeV from the nonrelativistic form-factor tabulations of Hubbel *et al.*¹⁴ and that the latter are a better approximation than the form factors obtained using relativistic wave functions.

C. Delbruck amplitudes

D scattering deals with the elastic scattering of photons from the Coulomb field of nuclei via real and virtual electron-positron production. Values of the D amplitudes were tabulated by Bar-Noy and Kahane¹⁵ using the theoretical formula given by Papatzacos and Mork¹⁶ and by Constantini.¹⁷ The D amplitudes for photon energies in the range $E = 4.0M-10.0$ MeV at $\theta = 1.0^\circ$ and 1.7° are listed in Table I and were calculated along the same lines mentioned above. The relative signs of the real and imaginary amplitudes appearing in the tables of Bar-Noy and Kahane have caused some confusion in the literature.⁹ This is due to the fact that the sign of the spin-flip ampli-

TABLE I. R amplitudes (in units of r_0) and D amplitudes (in units of $\alpha^2 Z^2 r_0$) used in calculating the theoretical cross sections at $\theta = 1.0^\circ$ and 1.7° . For complex R amplitudes, $A_{R2}^\perp = A_{R2}^\parallel \approx 0$.

E (MeV)	θ (deg)	$(\alpha^2 Z^2 r_0)$				(r_0)	
		A_{D1}^\perp	A_{D1}^\parallel	A_{D2}^\perp	A_{D2}^\parallel	$A_{R1}^\perp = A_{R1}^\parallel$	$Z=82$ $Z=83$
4.0	1.0	1.578	1.612	0.8682	0.8728	-10.48	-10.67
	1.7	1.450	1.506	0.8465	0.8587	-4.90	-4.99
4.5	1.0	1.825	1.873	1.141	1.150	-8.94	-9.20
	1.7	1.647	1.723	1.103	1.125	-4.30	-4.35
5.0	1.0	2.059	2.121	1.435	1.450	-7.72	-7.90
	1.7	1.823	1.921	1.372	1.408	-3.88	-3.92
5.5	1.0	2.276	2.357	1.745	1.768	-6.64	-6.80
	1.7	1.975	2.096	1.646	1.702	-3.52	-3.56
6.0	1.0	2.476	2.486	2.067	2.101	-5.81	-5.94
	1.7	2.105	2.250	1.920	2.000	-3.17	-3.22
6.5	1.0	2.657	2.780	2.396	2.445	-5.19	-5.29
	1.7	2.215	2.383	2.191	2.300	-2.83	-2.89
7.0	1.0	2.849	2.995	2.753	2.822	-4.73	-4.80
	1.7	2.305	2.495	2.455	2.598	-2.51	-2.57
7.5	1.0	2.966	3.134	3.062	3.153	-4.39	-4.45
	1.7	2.378	2.588	2.710	2.890	-2.22	-2.84
8.0	1.0	3.129	3.321	3.429	3.547	-4.11	-4.16
	1.7	2.436	2.663	2.955	3.176	-1.97	-2.02
8.5	1.0	3.206	3.421	3.721	3.869	-3.88	-3.93
	1.7	2.481	2.723	3.188	3.452	-1.75	-1.80
9.0	1.0	3.304	3.540	4.043	4.244	-3.66	-3.71
	1.7	2.513	2.768	3.409	3.718	-1.57	-1.62
9.5	1.0	3.388	3.645	4.357	4.575	-3.45	-3.50
	1.7	2.536	2.801	3.618	3.974	-1.42	-1.46
10.0	1.0	3.460	3.736	4.663	4.920	-3.25	-3.30
	1.7	2.549	2.822	3.814	4.218	-1.30	-1.33

^aThese amplitudes are related to the polarized ones appearing in Ref. 15 by $A_{D1}^\perp = \text{Re}M_{++} - \text{Re}M_{+-}$ and $A_{D1}^\parallel = \text{Re}M_{++} + \text{Re}M_{+-}$.

^bThose amplitudes are related to the ones appearing in Ref. 15 by $A_{D2}^\perp = \text{Im}M_{++} + \text{Im}M_{+-}$ and $A_{D2}^\parallel = \text{Im}M_{++} - \text{Im}M_{+-}$. The inconsistency in the two cases is discussed in the text (see Sec. III C).

tudes used by Papatzacos and Mork was different from that used by Constantini (see the footnote to Table I of the present work).

D. Nuclear resonance fluorescence scattering amplitude

The expression for A_F may be obtained by considering Fig. 2, which shows the overlap between the line shapes occurring in a photoexcitation process. In the figure, both the incident γ line, emitted by the $\text{Fe}(n, \gamma)$ reaction, and the resonance level in ^{208}Pb are Doppler broadened by thermal motion.

The Breit-Wigner scattering amplitude of a single photon of energy E incident on a nucleus of spin J_0 with an excited level of peak energy E_r , total width Γ , and spin J may be written (in units of r_0 , the classical electron radius) as follows (see Sec. III E):

$$A_F^\parallel(E, \theta) = A_{F1}^\parallel + iA_{F2}^\parallel = C_0 \frac{\Gamma/2}{(E_r - E) - i\Gamma/2} f_{\parallel}(\theta), \quad (5)$$

where

$$C_0 = \sqrt{\sigma_0}/r_0$$

and

$$\sigma_0 = 2\pi\lambda^2(2J+1)/(2J_0+1).$$

Since we are dealing with $M1$ dipole radiation¹⁸ (the 7.28 MeV level in ^{208}Pb is known to be 1^+) we therefore have

$$f_{\perp}(\theta) = \sqrt{3/8\pi}, \quad f_{\parallel}(\theta) = \sqrt{3/8\pi} \cos\theta, \quad A_F^\perp = A_F^\parallel \cos\theta. \quad (6)$$

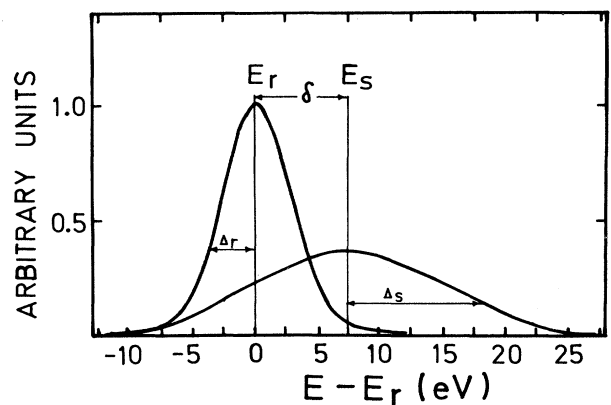


FIG. 2. Doppler-broadened line shapes of the incident γ line from the $\text{Fe}(n, \gamma)$ reaction of peak energy E_s and the resonance nuclear level (corrected for recoil energy) of peak energy E_r . The sign and magnitude of $\delta = E_s - E_r$ were determined by other experiments (Refs. 23 and 24).

In the following we ignore the angular dependence because at $\theta < 2^\circ$,

$$f_{\perp}(\theta) = f_{\parallel}(\theta) = f(\theta), \quad A_F^{\perp} = A_F^{\parallel}$$

and deal only with $f_{\parallel}(\theta)$ and A_F^{\parallel} .

In order to derive an expression for the elastic scattering cross section, one should first calculate the *coherent* superposition of the F process with other scattering processes. This coherent sum should be evaluated for *each incident photon* and then integrated incoherently over all photons, as explained in some detail below.

E. Elastic cross section

As mentioned above, the elastic cross section is obtained by using the amplitude A_F given by Eq. (5); we add it coherently to the other scattering amplitudes and obtain the value of $|A_{\parallel}|^2$ for this particular photon:

$$|A_{\parallel}|^2 = |A_F^{\parallel}(E, \theta, v) + A_S^{\parallel}(E, \theta, v)|^2, \quad (7)$$

with a similar expression for $|A_{\perp}|^2$.

A_S and A_F depend on the relative velocity v of the $\text{Fe}(n, \gamma)$ emitting nucleus with respect to the ^{208}Pb scatterer; the dependence of $A_S = A_D + A_R$ on v is very weak and may be taken as constant over the resonance region of width $\Delta E \sim 20$ eV. The incoherent sum may be calculated by integrating over all possible velocities v . If the velocity distribution is formally represented by a density function $\rho(v)$ [where $\int \rho(v) dv = 1$] the cross section may be written as

$$\begin{aligned} \frac{d\sigma}{d\Omega} &= \frac{r_0^2}{2} \int (|A_{\perp}|^2 + |A_{\parallel}|^2) \rho(v) dv \\ &= \frac{r_0^2}{2} \left\{ \int (|A_F^{\perp}|^2 + |A_F^{\parallel}|^2) \rho(v) dv + \{ |A_S^{\perp}|^2 + |A_S^{\parallel}|^2 \} \right. \\ &\quad \left. + 2 \sum_{j=1}^2 \left[A_{Sj}^{\perp} \int A_{Fj}^{\perp} \rho(v) dv + A_{Sj}^{\parallel} \int A_{Fj}^{\parallel} \rho(v) dv \right] \right\}. \end{aligned} \quad (8)$$

The last expression contains three terms: The first is identifiable with the differential scattering cross section $d\sigma_F/d\Omega$ of the pure F process, as it contains an integration over all possible relative velocities v (see Sec. III F). This term was also discussed in several earlier publications.^{7,8} The second term is the combined coherent differential scattering cross section $d\sigma_S/d\Omega$ of the D and R process, while the third is the interference term between the F and the other two processes. We may thus write

$$\begin{aligned} \frac{d\sigma}{d\Omega} &= \frac{d\sigma_F}{d\Omega} + \frac{d\sigma_S}{d\Omega} + r_0^2 [\bar{A}_{F1}(A_{S1}^{\perp} + A_{S1}^{\parallel}) \\ &\quad + \bar{A}_{F2}(A_{S2}^{\perp} + A_{S2}^{\parallel})], \end{aligned} \quad (9)$$

where A_{Sj}^{\perp} and A_{Sj}^{\parallel} were defined in Eq. (3) while $\bar{A}_{Fj} = \bar{A}_{Fj}^{\perp} = \bar{A}_{Fj}^{\parallel}$ ($j=1,2$) are the F scattering amplitudes averaged over all possible velocities v of the γ emitting nu-

cleus relative to the scattering nucleus and are evaluated in Sec. III F.

Since among all the γ lines of the $\text{Fe}(n, \gamma)$ reaction, only the 7.28 MeV line is resonantly scattered by ^{208}Pb , $\bar{A}_F \neq 0$ only at 7.28 MeV, while for all other γ lines $\bar{A}_F = 0$. Finally, we may account for the fact that in the present work a natural target was employed. Denoting the relative abundance of the ^{208}Pb isotope by P , the scattering cross section may be written as

$$\begin{aligned} \frac{d\sigma}{d\Omega} &= \frac{d\sigma_S}{d\Omega} + P \frac{d\sigma_F}{d\Omega} + r_0^2 P [\bar{A}_{F1}(A_{S1}^{\perp} + A_{S1}^{\parallel}) \\ &\quad + \bar{A}_{F2}(A_{S2}^{\perp} + A_{S2}^{\parallel})]. \end{aligned} \quad (10)$$

The quantity \bar{A}_F , the R and D scattering amplitudes (with the proper phase, see the next subsection) of the 7.28 MeV γ line resonantly scattered from ^{208}Pb , are listed in Table II. The values of the various quantities necessary for calculating \bar{A}_F (related to the 7.28 MeV resonant event) are listed in Table III.

F. Average F scattering amplitude

In order to calculate the effect of all relative velocities of the γ emitter with respect to the scatterer appearing in $\int A_F^{\parallel} \rho(v) dv$, we may proceed as follows: We use the laboratory system, and consider the scattering amplitude of Eq. (5). We then account for the effect of the thermal velocities of both the γ -emitting nuclei and the scattering nuclei on A_F . The effect of the Gaussian distribution of velocities of the scattering nuclei is given by

$$A_F^*(E) = C_0 C_1 f(\theta) \int_0^{\infty} \frac{e^{-(E-E')^2/\Delta_r^2}}{(E_r - E') - i\Gamma/2} dE', \quad (11)$$

where

$$C_1 = 1/\Delta_r \sqrt{\pi},$$

and

$$\Delta_r = E_r (2kT_r / M_r c^2)^{1/2}$$

is the Doppler width of the resonance level, M_r is the nuclear mass, and T_r is the effective temperature¹⁹ of the nuclear target. $A_F^*(E)$ may be evaluated to yield

$$A_F^*(E) = C_0 f(\theta) [-\chi(x, t) + i\psi(x, t)], \quad (12)$$

where the functions χ and ψ are given by

$$\chi(x, t) = \frac{1}{2\sqrt{\pi t}} \int_0^{\infty} y \frac{e^{-(x-y)^2/4t}}{1+y^2} dy, \quad (13)$$

$$\psi(x, t) = \frac{1}{2\sqrt{\pi t}} \int_0^{\infty} \frac{e^{-(x-y)^2/4t}}{1+y^2} dy, \quad (14)$$

with

$$t = (\Delta_r / \Gamma)^2$$

and

$$x = 2(E - E_r) / \Gamma.$$

TABLE II. A_D , A_R , A_S , and \bar{A}_F (in units of r_0) at 7278 keV from ^{208}Pb . A_S denotes the coherent sum of D and R amplitudes. The subscripts 1 and 2 denote the real and imaginary parts of the amplitudes. The imaginary R amplitudes are negligibly small.

θ	process	$(A^{\parallel})_1$	$(A^{\perp})_1$	$(A^{\parallel})_2$	$(A^{\perp})_2$
1.0°	Delbruck	1.1001	1.0434	1.0763	1.0472
	Rayleigh	-4.5303	-4.5310		
	A_S	-3.4302	-3.4876	1.0763	1.0472
	\bar{A}_F	-0.4884	-0.4884	+ 0.5711	+ 0.5711
1.7°	Delbruck	0.9126	0.8406	0.9888	0.9303
	Rayleigh	-2.3420	-2.3430		
	A_S	-1.4294	-1.5024	0.9888	0.9303
	\bar{A}_F	-0.4884	-0.4884	+ 0.5711	+ 0.5711

If we account for the fact that the incident γ line does not have a sharp energy E , but rather a Gaussian energy distribution determined by the thermal Doppler broadening of the (n, γ) source, we obtain for the average scattering amplitude

$$\bar{A}_F = C_0 C_2 f(\theta) \int_0^\infty A_F^*(E) e^{-[E - (E_r - \delta)]^2 / \Delta_s^2} dE, \quad (15)$$

which may be evaluated in a similar manner to that described in Ref. 20 to yield

$$\begin{aligned} \bar{A}_F &= \bar{A}_{F1} + i \bar{A}_{F2} \\ &= C_0 [-\chi(x_0, t_0) + i \psi(x_0, t_0)] f(\theta) \end{aligned} \quad (16)$$

with

$$\begin{aligned} t_0 &= (\Delta_r^2 + \Delta_s^2) / \Gamma^2, \\ x_0 &= \frac{2(E_s - E_r)}{\Gamma} = \frac{2\delta}{\Gamma}, \\ C_2 &= \frac{1}{\Delta_s \sqrt{\pi}}. \end{aligned}$$

It is very important to note that \bar{A}_F represents an *incoherent* normalized averaged sum over independent scattering amplitudes describing processes which occur when separate photons with a Gaussian energy distribution scatters from a Doppler-broadened nuclear level.

It should further be emphasized that \bar{A}_F is not a scattering amplitude in the normal sense because $r_0^2 |\bar{A}_F|^2$ is not equal to the differential scattering cross section $d\sigma_F/d\Omega$. This last quantity is given by

$$\frac{d\sigma_F}{d\Omega} = \frac{r_0^2}{2} \int \{ |A_F^{\parallel}(E, \theta)|^2 + |A_F^{\perp}(E, \theta)|^2 \} \rho(v) dv. \quad (17)$$

The last integral is in effect a convolution of the Breit-Wigner cross section with the thermal Doppler broadening

TABLE III. The parameters of the 7.278 MeV resonance in ^{208}Pb .

$\Gamma = \Gamma_0 = 0.78$ eV	$\delta = +7.3$ eV
$\Delta_r = 3.76$ eV	$x_0 = 18.72$
$\Delta_s = 10.44$ eV	$t_0 = 123.7$
$\sigma_0 = 138.6$ mb	$\psi(x_0, t_0) = 0.03954$
$\sigma_F = 5.56$ b	$\chi(x_0, t_0) = 0.03381$
$P = 0.523$	

of both the γ emitting and the scattering nuclei. It can be calculated by following exactly the same steps as that given in Eqs. (11)–(16), thus yielding

$$\begin{aligned} \frac{d\sigma_F}{d\Omega} &= \frac{3}{8\pi} \left[\frac{1 + \cos^2\theta}{2} \right] \sigma_0 \psi(x_0, t_0) \\ &= \frac{3}{8\pi} \left[\frac{1 + \cos^2\theta}{2} \right] \sigma_F, \end{aligned} \quad (18)$$

where σ_0 , x_0 , and t_0 were given in Eqs. (5) and (16).

G. Phase relations

The problem of the relative phases of the imaginary and the real parts of the amplitudes for the D , R , N , and T scattering processes was discussed in detail in earlier publications^{10,16} and could be summarized as follows:

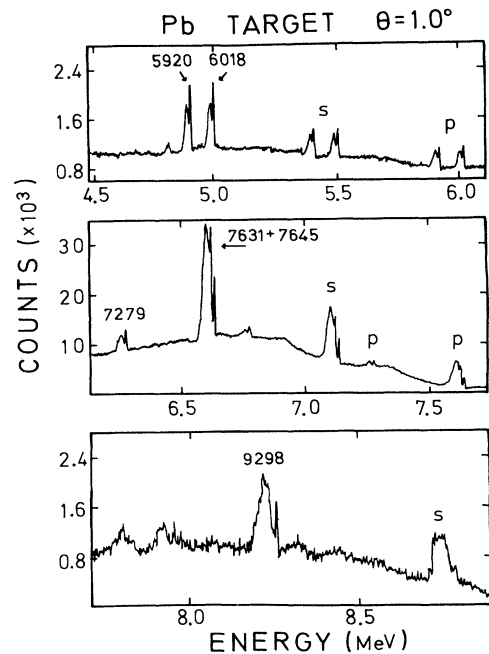


FIG. 3. Typical scattered spectrum from a Pb target at $\theta = 0.95^\circ \pm 0.07^\circ$ showing a broad Compton peak near each narrow elastic peak. The γ source was obtained from the $\text{Fe}(n, \gamma)$ reaction. P and S denote photopeaks and first escape peaks; other lines denote second escape peaks.

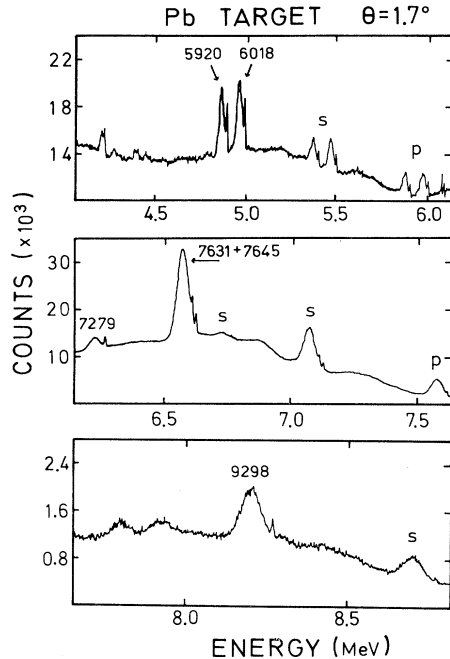


FIG. 4. Scattered spectrum from a Pb target at $\theta = 1.69^\circ \pm 0.02^\circ$. See the caption to Fig. 3.

(1) All the imaginary amplitudes at $\theta = 0^\circ$ are positive, as is immediately obvious from the optical theorem

$$\text{Im}A(E, \theta = 0^\circ) = \frac{E}{4\pi\hbar c} \sigma_a(E), \quad (19)$$

where $\sigma_a(E)$ is the absorption cross section of the corresponding absorption process, which is always positive.

(2) The sign of the real part of the amplitude is positive or negative according to whether $\sigma_a(E)$ is an increasing or decreasing function of energy. For the F amplitude we use the same sign convention as that obtained for A_N , that being the nuclear resonance scattering amplitude²¹ from the GDR. This choice may be easily shown to be consistent with causality arguments discussed by Gell-Mann *et al.*²² From the above, it follows that in a random pho-

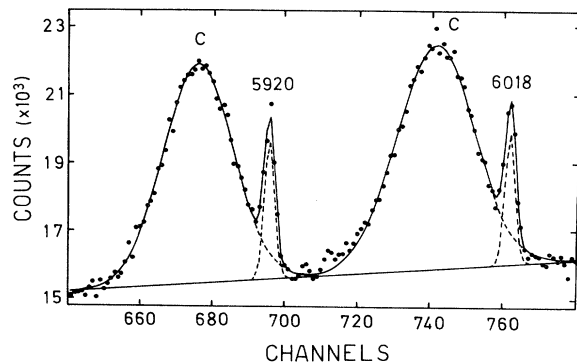


FIG. 5. Typical results of curve fitting of skew Gaussians to the elastic and Compton peaks. The procedure is shown for the double escape peaks of the 5920 and 6018 keV γ lines scattered at $\theta = 1.7^\circ$ from a Bi target.

TABLE IV. Values of the incoherent scattering function S (taken from Ref. 14) at various photon energies.

E (keV)	S			
	$\theta \sim 1^\circ$		$\theta = 1.7^\circ$	
	$Z = 82$	$Z = 83$	$Z = 82$	$Z = 83$
4406			73.65	75.23
4810			74.64	76.30
5920	70.72	72.84	77.56	78.43
6018	70.96	73.06	77.69	78.56
7278	73.49	75.51	78.99	79.91
7631 + 7646	74.10	76.07	79.26	80.18
9298	76.30	78.15	80.10	81.05

toexcitation process (as that depicted in Fig. 2), the sign of the imaginary part of A_F is positive and that of the real part of A_F is negative. This is because the peak energy E_s of the incident photons is known to be larger^{23,24} than the peak energy E_r of the resonance level. This fact, namely, $E_s - E_r = \delta > 0$ (for the specific case of the 7.28 MeV γ line scattered by ^{208}Pb) was determined by two independent methods, by using a rotor²³ and by measuring the nuclear self-absorption²⁴ at small scattering angles $\theta \leq 15^\circ$. In this connection, it should be remarked that the magnitude of $|\delta|$ is usually determined by a temperature-variation measurement.¹

The result of the above experiments was

$$\delta = +7.3 \pm 0.3 \text{ eV}.$$

It is important to note that in a resonance scattering event where $\delta = 0$ (i.e., when the incident γ line overlaps exactly the resonance level), one finds $\bar{A}_F = 0$, and hence the net interference effect is zero. In this case, the superposition of the F process and the D and R scattering yields the incoherent sum as in Eq. (10). The above discussion also indicates, for the first time, that the sign of δ is of physical significance, namely, a positive δ yields a constructive interference with D and R scattering, while a negative δ yields destructive interference at $\theta = 1.0^\circ$ and 1.7° .

IV. RESULTS

Figures 3 and 4 show the spectra of the high energy part of the scattered radiation from a Pb target at $\theta = 1.0^\circ$ and 1.7° , respectively. Both spectra reveal the interesting feature that besides each narrow elastic peak there is a neighboring large broad inelastic Compton peak. As noted in Ref. 6, the appearance of the two peaks served three purposes: (1) to determine the absolute elastic differential cross section from the measured ratios of areas of the elastic to Compton peaks by employing the theoretically calculated Compton cross sections; (2) to find the scattering angle θ from the energy separation between the elastic and the Compton peak; and (3) to determine the angular spread $\Delta\theta$ from the width and shape of the Compton peak.

The extraction of the ratios of the elastic to Compton peaks was carried out using a computer code which fitted skew Gaussians²⁸ of variable width to both the elastic peak and the Compton peaks. Figure 5 shows a typical

TABLE V. Measured elastic differential cross sections of photons in units of b/sr scattered from Pb and Bi at $\theta=1^\circ$ and 1.7° .

E (keV)	$\theta=1.0^\circ$		$\theta=1.7^\circ$	
	Pb (b/sr)	Bi (b/sr)	Pb (b/sr)	Bi (b/sr)
4218	4.36±0.61	4.97±1.25	1.43±0.11	1.86±0.24
4406			1.14±0.15	1.05±0.20
4810			0.72±0.12	0.86±0.30
5920	1.88±0.10	1.98±0.33	0.60±0.03	0.58±0.02
6018	1.89±0.13	1.85±0.10	0.51±0.01	0.47±0.01
7278	1.49±0.08	0.64±0.08	0.66±0.03	0.26±0.01
7631 + 7645	1.03±0.04	0.93±0.04	0.23±0.02	0.21±0.03
9298	0.46±0.07	0.36±0.20	0.17±0.01	0.17±0.01

result of such a separation for the second escape peaks of the 5920 and 6018 keV lines scattered from a Bi target at $\theta=1.7^\circ$.

The shape of the Compton peak may also be determined by using carbon or aluminum targets (containing the same numbers of electrons as that of the high- Z scatterer) and measuring the resulting scattered spectrum. Obviously the C target produces no elastic peak and the scattered radiation is the result of the Compton scattering of carbon plus the edge effects of the collimators and absorber.

The Compton scattering cross section $d\sigma_C/d\Omega$ was calculated by multiplying the Klein-Nishina value $d\sigma_{KN}/d\Omega$ by the incoherent scattering function¹⁴ S :

$$\frac{d\sigma_C}{d\Omega} = S \frac{d\sigma_{KN}}{d\Omega}.$$

It may be noted that the Klein-Nishina cross section is

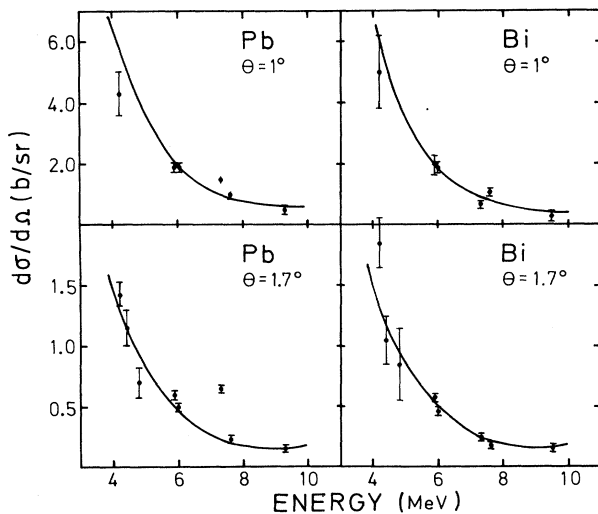


FIG. 6. Differential cross sections for elastic scattering of photons from Pb and Bi at $\theta=1^\circ$ and 1.7° . The curves are obtained by reducing the R amplitudes by 5%, resulting in a better fit at the higher energies. The contribution of NRF scattering is not included.

correct only for free electrons at rest, and the factor S takes into account the effect of bound electrons in cases where the recoil energy of the Compton scattered electrons is smaller than the binding energy. The values of S , taken from Hubbel *et al.*,¹⁴ are listed in Table IV.

The measured elastic cross sections extracted from the experimental area ratios are given in Table V for both Pb and Bi targets at $\theta=1.0^\circ$ and 1.7° for several γ lines in the energy range 4.0–10 MeV. These results together with predicted values are presented graphically in Fig. 6.

V. DISCUSSION

A. Rayleigh and Delbruck scattering

In the following, we deal only with *nonresonant* scattering events in order to find out to what extent the predicted elastic scattering cross sections (obtained using the D and R amplitudes of Table I) agree with the experimental results. In carrying out this comparison we considered only the results of γ lines at 4.406, 4.810, 5.920, 6.018, and 9.298 MeV. Thus, we excluded the results of the γ lines at 7.28 MeV and 7.632 + 7.646 MeV. This is because the first line is known to yield a strong resonance scattering signal¹ in ^{208}Pb and a weak resonant signal²⁵ in ^{209}Bi . The other two lines are known to hit upon strong neutron-emitting levels in ^{207}Pb and ^{208}Pb , respectively^{26,27} while in Bi, the 7.646 MeV γ line is known to produce resonance neutrons through the (γ, n) reaction. It was found that the predicted cross section obtained using Table I overestimated the measured results and that it is necessary to reduce the R amplitudes at $\theta=1^\circ$ by $\sim 5\%$ to achieve a better agreement with experiment for photon energies

TABLE VI. Measured and theoretical cross sections of the 7278 keV line scattered from natural Pb (in mb/sr). Values of the three terms appearing in Eq. (10) are also given.

	$\theta=1.0^\circ$	$\theta=1.7^\circ$
$d\sigma/d\Omega$ (meas)	1490±80	663±30
$d\sigma_S/d\Omega$	920	244
$P d\sigma_F/d\Omega$	347	347
Interference	182	105
$d\sigma/d\Omega$ (calc)	1449	696

where nonresonant scattering occurs.

The 5% reduction in the R amplitudes may be justified by noting that the contribution of the L - and M -shell electrons is overestimated in the modified form factor approximation,¹¹ and that this deviation increases towards small momentum transfers. Thus, this 5% correction was applied only at the smaller angle, $\theta=1^\circ$. It may be noted that the effect of this correction on the scattering cross section is large only at small E because the relative contribution of R scattering decreases with increasing E .

B. Constructive interference between $(R+D)$ and F processes

In order to find whether there is evidence for an interference effect between $(R+D)$ and the F process, we first consider the magnitude of the three terms [Eq. (10)] constituting the elastic scattering cross section from the 7.28 MeV level in ^{208}Pb . It may be seen from the numerical values of these terms (Table VI) that the relative magnitude of the interference term is only about 15% of the incoherent combined contribution of F and $(R+D)$ scattering. Thus a precise knowledge of each of the first two terms of Eq. (10) is necessary before any conclusion could be drawn concerning the contribution of the interference term. The magnitude of the F scattering is determined to within 5% accuracy from an independent measurement at backward angles.¹ The second term, namely $(D+R)$ scattering, was discussed in the preceding section, where it was found that it is necessary to reduce the R amplitudes by 5% to achieve an overall good agreement between experiment and predicted values.

From Table VI, it is clear that the *incoherent* sum of the F and $(D+R)$ cross section is smaller than the measured value at $\theta=1^\circ$ and 1.7° . In addition, only by including the interference term is a good agreement between the measured and predicted values obtained. Hence those results constitute for the first time definite evidence for the existence of a *constructive* interference between $(D+R)$ and F processes.

It may be seen from a consideration of the signs of the various scattering amplitudes that the real D amplitude has an opposite sign to that of the real part of both the R and the F processes. Therefore, one would expect that at larger scattering angles, namely at $\theta \geq 5^\circ$, where the contribution of D scattering is dominant, *destructive* interference should result between $(R+D)$ scattering and F . Such a measurement, at $\theta \geq 5^\circ$, is very difficult because the scattering cross section decreases with increasing θ , and a new design of absorber and collimators is required before performing such a measurement. It should be added that destructive interference may also occur when a target having a scattering event with negative value of δ is used at small scattering angles where the R contribution is dominant.

ACKNOWLEDGMENTS

One of us (R.M.) would like to thank Professor Y. Aharonov and Professor Y. Avishai for helpful discussions concerning the derivation of the scattering amplitudes. S. K. would like to thank Professor R. H. Pratt for illuminating discussions concerning the Rayleigh amplitudes.

-
- ¹R. Moreh, S. Shlomo, and A. Wolf, Phys. Rev. C **2**, 1144 (1970).
²R. Moreh, I. Jacob, and R. Mourad, Nucl. Instrum. Methods **127**, 193 (1975).
³S. Kahane and R. Moreh, Phys. Rev. C **9**, 2384 (1974).
⁴Z. Berant, R. Moreh, and S. Kahane, Phys. Lett. **69B**, 281 (1977).
⁵Z. Berant and R. Moreh, Phys. Lett. **73B**, 142 (1978).
⁶S. Kahane, R. Moreh, and O. Shahal, Phys. Rev. C **18**, 1217 (1978); Phys. Lett. **66B**, 229 (1977).
⁷B. Arad and G. Ben-David, Rev. Mod. Phys. **45**, 230 (1973).
⁸R. Moreh, Nucl. Instrum. Methods **166**, 69 (1979).
⁹P. Rullhusen *et al.*, Nucl. Phys. **A382**, 79 (1982).
¹⁰R. Moreh, Nucl. Instrum. Methods **166**, 91 (1979).
¹¹L. Kissel, R. H. Pratt, and S. C. Roy, Phys. Rev. A **22**, 1970 (1980); L. Kissel and R. H. Pratt, Phys. Rev. Lett. **40**, 387 (1978).
¹²G. E. Brown and D. F. Mayers, Proc. R. Soc. London Ser. A **242**, 89 (1957).
¹³D. A. Liberman, D. T. Cromer, and J. T. Waber, Comput. Phys. Commun. **2**, 107 (1971).
¹⁴J. H. Hubbel *et al.*, J. Phys. Chem. Ref. Data **4**, 471 (1975).
¹⁵S. Kahane and T. Bar-Noy, Nucl. Phys. **A288**, 132 (1977).
¹⁶P. Papatzacos and K. Mork, Phys. Rev. D **12**, 206 (1975); Phys. Rep. **21C**, 81 (1975).
¹⁷V. Constantini, B. de Tollis, and G. Pistoni, Nuovo Cimento **2A**, 733 (1971).
¹⁸R. Moreh and M. Friedman, Phys. Lett. **26B**, 579 (1968); **31B**, 642 (E) (1970).
¹⁹W. E. Lamb, Phys. Rev. **55**, 190 (1939).
²⁰B. Arad, G. Ben-David, I. Pelah, and Y. Schlesinger, Phys. Rev. **133**, B684 (1964).
²¹E. G. Fuller and E. Hayward, Nucl. Phys. **30**, 613 (1962).
²²M. Gell-Mann, M. L. Goldberger, and W. E. Thirring, Phys. Rev. **95**, 1612 (1954).
²³B. Arad, G. Ben-David, and Y. Schlesinger, Phys. Rev. **136**, B370 (1964).
²⁴J. A. McIntyre and J. D. Randall, Phys. Lett. **17**, 137 (1965).
²⁵I. Jacob, R. Moreh, and A. Wolf, Nucl. Phys. **A291**, 1 (1977).
²⁶R. Moreh, Y. Birenbaum, and Z. Berant, Nucl. Instrum. Methods **155**, 429 (1978).
²⁷Y. Birenbaum *et al.*, Nucl. Phys. **A369**, 483 (1981).
²⁸G. W. Phillips and K. W. Marlow, Nucl. Instrum. Methods **137**, 525 (1976).